Phase-resolved acoustic radiation force optical coherence elastography

Wenjuan Qi,[a,b] Ruimin Chen,[c] Lidek Chou,[a] Gangjun Liu,[a] Jun Zhang,[a] Qifa Zhou,[c] and Zhongping Chen[a,b,d]
[a]University of California, Irvine, Beckman Laser Institute, Irvine, 1002 Health Sciences Road East, California 92612
[b]University of California, Irvine, Department of Chemical Engineering and Materials Science, California 92697
[c]University of Southern California, Department of Biomedical Engineering, NIH Ultrasonic Transducer Resource Center, Los Angeles, California 90089
[d]University of California, Irvine, Department of Biomedical Engineering, California 92697

Abstract. Many diseases involve changes in the biomechanical properties of tissue, and there is a close correlation between tissue elasticity and pathology. We report on the development of a phase-resolved acoustic radiation force optical coherence elastography method (ARF-OCE) to evaluate the elastic properties of tissue. This method utilizes chirped acoustic radiation force to produce excitation along the sample's axial direction, and it uses phase-resolved optical coherence tomography (OCT) to measure the vibration of the sample. Under 500-Hz square wave modulated ARF signal excitation, phase change maps of tissue mimicking phantoms are generated by the ARF-OCE method, and the resulting Young's modulus ratio is correlated with a standard compression test. The results verify that this technique could efficiently measure sample elastic properties accurately and quantitatively. Furthermore, a three-dimensional ARF-OCE image of the human atherosclerotic coronary artery is obtained. The result indicates that our dynamic phase-resolved ARF-OCE method can delineate tissues with different mechanical properties. [DOI: 10.1117/1.JBO.17.11.110505]

Keywords: optical coherence tomography; elastography; acoustic radiation force; Young's modulus; mechanical properties; atherosclerosis.

Paper 12382L received Jun. 21, 2012; revised manuscript received Sep. 24, 2012; accepted for publication Sep. 26, 2012; published online Nov. 2, 2012.

1 Introduction

Many diseases involve change in the biomechanical properties of tissue. Cancerous tumors usually appear as hard nodules, and their stiffness differs from the surrounding tissue.[1] A calcified plaque is markedly stiffer than the microenvironment around it. Elastography, quantitatively interrogating tissue mechanical properties by applying force to the tissue, has attracted increasing research interest. The beauty of elastography is that it is capable of delineating tissues with different mechanical properties even when their structures appear very similar. Magnetic resonance elastography and ultrasonic elastography are two mature imaging modalities being used for measuring mechanical properties at the tissue and organ level. Optical coherence elastography (OCE),[2–6] like all forms of optical coherence tomography (OCT), has a superior micrometer scale resolution and is therefore suitable for imaging subtle mechanical changes in the early stages of disease.

Excitation and detection are generally two characteristics of an OCE system. OCE falls into two main categories with respect to the excitation method: static/quasi-static excitation OCE[2–4] and dynamic excitation OCE.[5–7] The former applies compression to the subject statically/quasi-statically and measures the relaxation dynamics, whereas the latter dynamically excites the subject using various waveforms and detects the induced displacement in a gated time window, which enables a much higher imaging speed. The recent reported dynamic OCE, featuring in direct-contact mechanical excitation method and a 5-kHz line rate, is applied for three-dimensional (3-D) skin imaging.[7] In terms of the detection method, there are two widely used algorithms: speckle tracking and the phase-resolved method. In comparison with the speckle tracking algorithm, which suffers from low accuracy due to decorrelation, the phase-resolved method provides sensitive displacement measurement at nanometer resolution. This is especially important for intravascular imaging, because better sensitivity in displacement measurement minimizes the force that must be applied to a vessel wall to quantify tissue mechanical properties. Phase-resolved OCE had been investigated previously for shear wave/surface acoustic wave (SAW) propagation detection,[8,9] but this method requires separation between excitation and detection points, which limits the speed and spatial resolution. Adaptation of this method is difficult for *in vivo* real-time two-dimensional (2-D) and 3-D vascular elastography.

In this paper, we propose a dynamic phase-resolved acoustic radiation force optical coherence elastography (ARF-OCE) method, which is capable of high-speed, high-spatial-resolution, point-by-point elastogram mapping in the axial direction. By applying a modulated acoustic radiation force to the sample and detecting the phase induced by the vibration of the sample using the phase-resolved OCT method, ARF-OCE is able to determine the relative Young's modulus in various phantoms and human coronary artery tissues. The high-speed and high-spatial-resolution phase-resolved ARF-OCE has the potential to measure tissue elasticity (Young's modulus) *in vivo* quantitatively.

2 Materials and Methods

2.1 *Tissue Phantom and Tissue Preparation*

The side-by-side agarose tissue phantom was fabricated. Two different concentrations of agarose (3.5% and 7% weight/volume) were used to obtain two different Young's moduli in each side of the phantom. The 3-mm-thick sample was sectioned for OCE imaging.

A section of postmortem human atherosclerotic coronary artery was obtained and stored at 0°C. The tissue was cut open and flattened prior to the ARF-OCE imaging.

2.2 *ARF-OCE System*

An 890-nm spectral-domain OCT system with a 20-kHz acquisition rate, as shown in Fig. 1, was used for vibration detection. The axial and lateral resolutions of the system were measured to

Address all correspondence to: Zhongping Chen, University of California, Irvine, Beckman Laser Institute, 1002 Health Sciences Road East, California 92612. Tel: 949-824-1247; Fax: 949- 824-8413; E-mail: z2chen@uci.edu

0091-3286/2012/$25.00

be 3.5 and 14.8 μm, respectively. The signal-noise-ratio (SNR) of the system was 100 dB with 650 μW of sample arm power and a 50-μs A-line rate. The minimum detectable phase for this system was measured to be 1.5 mrad, which corresponded to a velocity sensitivity of 2.13 μm/s. For the purposes of elastography, the sample was placed on the surface of a focused ultrasonic transducer, where the acoustic force was measured as roughly uniform by a highly accurate hydrophone. The transducer featured a resonant frequency of 4 MHz and was driven by a square wave modulated RF signal (50% duty cycle amplitude modulation) to generate periodical acoustic radiation pushes in the longitudinal direction on to the sample through a thin layer of ultrasound gel. The modulation frequency and amplitude were chosen for each sample in such a way that the phase difference induced between adjacent A-lines was large, to enhance the sensitivity, but less than $|\pi|$, to avoid phase wrapping. The phase difference was obtained from consequent A-lines while the system was scanning continuously. The oversampled data points were averaged by a factor of 4 and then used to calculate the phase shift for each A-line. From the phase shift information, the instantaneous axial velocity can be extracted as

$$v(x,z,t) = \Delta\phi(x,z,t)\lambda_0/4\pi n\tau, \tag{1}$$

where the light source center wavelength λ_0 is 890 nm, and the adjacent A-line time interval τ is 50 μs. x and z represent the lateral and axial location, $\Delta\phi$ denotes the phase shift between two adjacent A-lines, and n is the tissue refraction index, which is assumed to be 1.4 in this paper. Within a certain customized time window, the displacement Δd and the axial strain ε of the sample are expressed as

$$\Delta d = \int_{t_1}^{t_2} \frac{\Delta\phi(x,z,t)\lambda_0}{4\pi n\tau}\,\mathrm{d}t \tag{2}$$

$$\varepsilon = \int_{t_1}^{t_2} \frac{\Delta\phi(x,z,t)\lambda_0}{4\pi n\tau z_0}\,\mathrm{d}t, \tag{3}$$

where z_0 is the original thickness of the sample prior to ultrasonic stimulation. Young's modulus is an important parameter that characterizes the elastic properties of the sample. It is defined by

$$E = \frac{\sigma}{\varepsilon} = \frac{F/A}{\varepsilon}, \tag{4}$$

where σ is the axial (or normal) stress (force per area) acting on the sample, F is the acoustic radiation force out of the ultrasonic transducer, and A is the sample surface area. Since the acoustic radiation force was uniform and the OCT probe beam size is much less than the ultrasound beam waist, the strain applied in the experiment is small enough (less than 0.1) that the material can be assumed as elastic, and Eq. (4) can be used as the first-order approximation to quantify the relative dynamic Young's modulus in our dynamic OCE method. In this experiment, ARF-OCE of both the phantom and the human coronary artery samples were constructed while the samples were under vibration excitation.

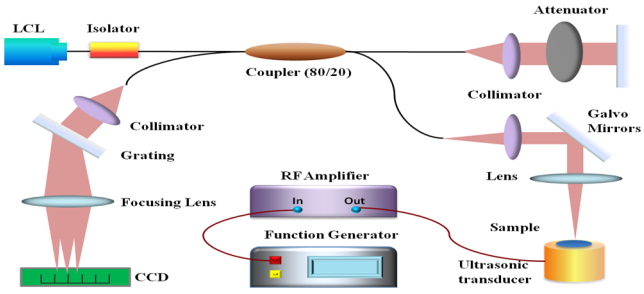

Fig. 1 Schematic diagram of the spectral-domain ARF-OCE system.

3 Results and Discussion

The feasibility of the ARF-OCE system was first tested on a side-by-side agarose phantom. An OCE image was acquired on the sample with 2048 A-lines over a scanning length of 6 mm. A B-mode OCT image of the phantom, in which the two sides of different concentration agarose cannot be clearly distinguished, is shown in Fig. 2(a). The phase shift between two successive A-lines was calculated using the phase-resolved method, and the resultant phase maps of the OCE image of the phantom are presented in Fig. 2(b) and 2(c). The displacement of the sample over time is proportional to the adjacent A-line phase shift at each lateral location and is calculated according to Eq. (2). As shown in Fig. 2(b) and 2(c), the boundary (red arrow) between the different concentrations of agarose in the phantom is clear in the OCE image, which demonstrates the advantage of OCE over OCT intensity imaging. The displacements of the two sides were 2.291 and 0.748 μm, respectively, which corresponded to 0.076% and 0.025% ARF induced strain, given the thickness of each side of the phantom was 3 mm. Because the radiation force was distributed equally in the region of interest, a 1:3.05 Young's modulus ratio between the two sides of the phantom was obtained according to Eq. (4). The Young's modulus of the agarose phantom was also measured under a compression test (MTS Synergie 100). The Young's moduli for 3.5% and 7% agarose samples were 83.6 and 265.7 kPa, respectively. The results of the two methods agree with each

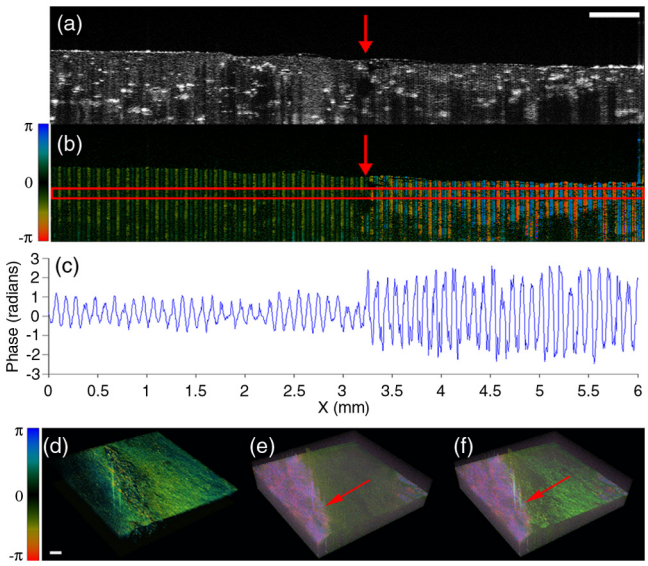

Fig. 2 (a) OCT intensity image of side-by-side agarose phantom. (b) The OCE image clearly reveals the boundary of the phantom when 500-Hz, 200-mV square wave modulated excitation was applied to the phantom. (c) Phase amplitude image. Red arrows indicate the boundary between the two sides, which differ in agarose concentration. (d) 3-D OCT, (e) AF-OCE, and (f) fused OCT and AF-OCE images of an agarose tissue-mimicking phantom. The phantom is excited with a 500-Hz square wave modulated RF signal. Scale bars: 500 μm.

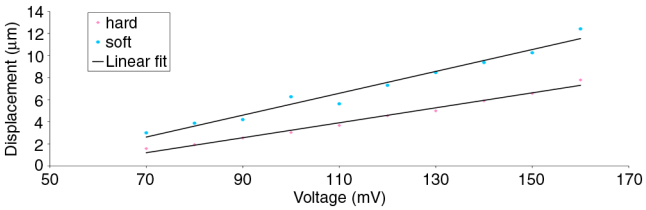

Fig. 3 Axial displacement as a function of preamplified voltage to the transducer.

other very well; the Young's modulus of the 7% agarose sample is also triple the one for the 3.5% sample, which indicates that our ARF-OCE method is capable of quantitatively characterizing the mechanical properties of sample materials. Figure 2(d)–2(f) shows the three-dimensional ARF-OCE performed on the agarose tissue phantom with 7% agarose on the right and 3.5% on the left. In the 3-D OCT image, shown in Fig. 2(d), it is difficult to differentiate the two sides of the phantom with different stiffness. However, the 3-D ARF-OCE image, shown in Fig. 2(e), clearly delineates the two materials, which differ in their stiffness. The color difference indicates different vibration levels. The pink color indicates a stronger vibration level, and the green-black color represents stiffer material, which vibrates more weakly under the same excitation. This result confirms our method's capacity to provide an additional and effective contrast in material stiffness.

To test the consistency of this method, we determined the displacement as a function of applied voltage, which is proportional to the acoustic radiation force out of the ultrasonic transducer (shown in Fig. 3). Both the hard and the soft samples acted linearly when the applied voltage increased. The Young's modulus ratio was calculated as the average value of the ratio between two samples under each voltage. A 1 : 1.74 ratio was given by the phase-resolved ARF-OCE measurement, which agrees with the 1 : 1.83 ratio from the standard compression test.

To demonstrate the potential of this technology in intravascular imaging, we have performed imaging of a section of atherosclerotic human cadaver coronary artery with the phase-resolved ARF-OCE (Fig. 4). An OCT intensity image, shown in Fig. 4(a), provided a general morphological view of the tissue, but no obvious evidence of atherosclerosis was found. However, in Fig. 4(b), a strong vibration phase contrast could be clearly imaged using ARF-OCE. The red-colored region indicated by the blue arrow in the ARF-OCE image is characterized by smaller phase and less vibration and, therefore, represents less elastic, stiffer tissue such as plaques. The stronger vibration representing softer tissue (dark area) is indicated by yellow arrows. In this ARF-OCE image, the stiffer tissue, corresponding to the atherosclerotic lesion in the blue box in the histological image [Fig. 4(c)], is clearly distinguishable from the softer (normal) tissue area. The transition between plaque and normal regions appears orange in color (indicated by the red arrow) and is characterized by intermediate elasticity. This preliminary result clearly shows that our ARF-OCE method has great potential to characterize tissue mechanical properties quantitatively and thereby delineate diseased tissue from normal tissue.

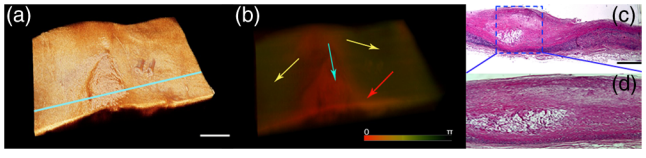

Fig. 4 (a) OCT structural and (b) ARF-OCE phase images of a human cadaver coronary artery under 500-Hz, 350-mV AM modulated excitation; an atherosclerotic lesion was identified as the red region corresponding to the blue box in (c) the histological image [corresponding to across blue line location in (a)] and (d) the close-up view of the atherosclerotic lesion. Scale bars: 1 mm.

4 Conclusion

We have developed a dynamic phase-resolved ARF-OCE method for accessing tissue mechanical properties along the axial direction. The feasibility of the method was first tested on different tissue-mimicking phantoms. The ratio of Young's moduli of 3.5% and 7% agarose concentration phantoms obtained from the aforementioned method corresponded very closely with the standard compression test result. Measurements using this method were also confirmed to be consistent by analyzing displacement under varying radiation forces. We have performed *in vitro* imaging of an atherosclerotic human cadaver coronary artery specimen with ARF-OCE. The atherosclerosis was found in the ARF-OCE image, while no obvious evidence appeared in the OCT image. This result shows that our ARF-OCE method has great potential to delineate diseased tissue from normal tissue and quantitatively characterize mechanical properties of tissues.

Acknowledgments

The authors thank Claire Robertson for the phantom compression test, Jiawen Li for preparing the tissue, and the individuals who donated their bodies and tissues for the advancement of education and research. This work was supported by the National Institutes of Health (EB-10090, EY-021519, HL-105215, HL-103764, and EB-015890), the Air Force Office of Scientific Research (FA9550-04-0101), and the Arnold and Mabel Beckman Foundation. Dr. Chen has a financial interest in OCT Medical Imaging Inc., which, however, did not support this work.

References

1. B. S. Garra et al., "Elastography of breast lesions: initial clinical results," *Radiology* **202**(1), 79–86 (1997).
2. J. Rogowska et al., "Optical coherence tomographic elastography technique for measuring deformation and strain of atherosclerotic tissues," *Heart* **90**(5), 556–562 (2004).
3. R. K. Wang, S. Kirkpatrick, and M. Hinds, "Phase-sensitive optical coherence elastography for mapping tissue microstrains in real time," *Appl. Phys. Lett.* **90**(16), 164105 (2007).
4. S. G. Adie et al., "Spectroscopic optical coherence elastography," *Opt. Express* **18**(25), 25519–25534 (2010).
5. X. Liang et al., "Dynamic spectral-domain optical coherence elastography for tissue characterization," *Opt. Express* **18**(13), 14183–14190 (2010).
6. R. K. Wang, Z. Ma, and S. J. Kirkpatrick, "Tissue Doppler optical coherence elastography for real time strain rate and strain mapping of soft tissue," *Appl. Phys. Lett.* **89**(14), 144103 (2006).
7. B. F. Kennedy et al., "*In vivo* three-dimensional optical coherence elastography," *Opt. Express* **19**(7), 6623–6634 (2011).
8. M. Razani et al., "Feasibility of optical coherence elastography measurements of shear wave propagation in homogeneous tissue equivalent phantoms," *Biomed. Opt. Express* **3**(5), 972–980 (2012).
9. C. Li et al., "Quantitative elastography provided by surface acoustic waves measured by phase-sensitive optical coherence tomography," *Opt. Lett.* **37**(4), 722–724 (2012).